

Pushing the Limits of LiDAR: Accurate Performance Analysis of Indoor 3D LiDARs

Supplementary Material

In this appendix, we provide supplementary information to support our indoor LiDAR performance analysis research. This chapter begins with an overview of the dataset and arm length calibration. We then present various analytical visualizations, including histograms, accuracy, and precision, followed by an examination of chessboard test results. Finally, we offer instructions for utilizing the dataset.

7.1. Dataset Description

7.1.1 Dataset Overview

The dataset is an extensive compilation of LiDAR scans from four models, accompanied by high-precision ground truth data. Table 7 provides a summary of the dataset.

LiDAR Model	Static Scans	Total Points	Size (GB)
Hesai PandarQT64	8,544	304M	48.5
Hesai PandarXT32	8,255	514M	74.1
Ouster OS0-128 Rev6	8,319	1,020M	148.4
Ouster OS0-128 Rev7	8,106	1,025M	147.3

Table 7. Dataset Summary

7.1.2 Data Collection Environment

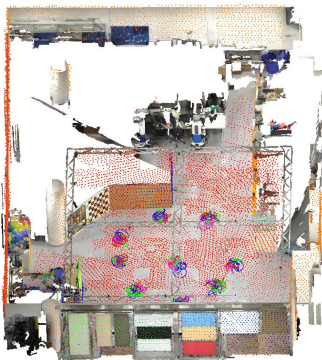


Figure 10. Test Environment Layout

The test environment was designed to include a wide range of materials and geometries commonly found in indoor settings. Figure 10 and Figure 11 illustrate the test area, including a FARO mesh ground truth model, annotated LiDAR point clouds, and the sensor position of each LiDAR. For better visualization, the ceiling of the mesh model was removed, and the labeled LiDAR pointclouds were downsampled to a resolution of 0.1 meters.

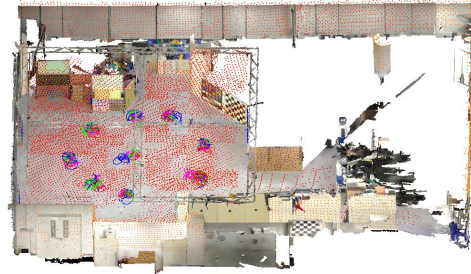


Figure 11. Test Environment Layout

7.2. Arm Length Calibration

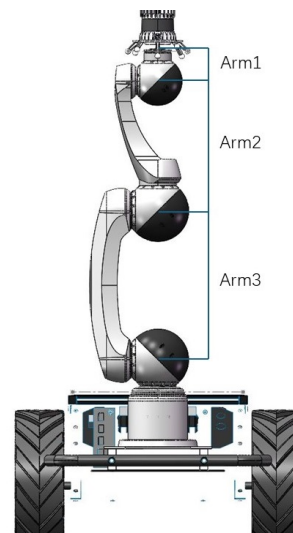


Figure 12. Robotic arm setup with LiDAR mount on Robot Platform

Figure 12 depicts the CAD of our robotic arm, encompassing the robot platform, the LiDAR mount, and OptiTrack markers. Each ball represents a joint of the arm, with three arm lengths requiring calibration.

During calibration, each joint was rotated to describe a circular path, with OptiTrack markers recording the positions throughout the motion. The arm lengths were then calculated by fitting a circle to the recorded data, as shown in Figure 13, where colored points represent OptiTrack data and the black line indicates the fitted circle.

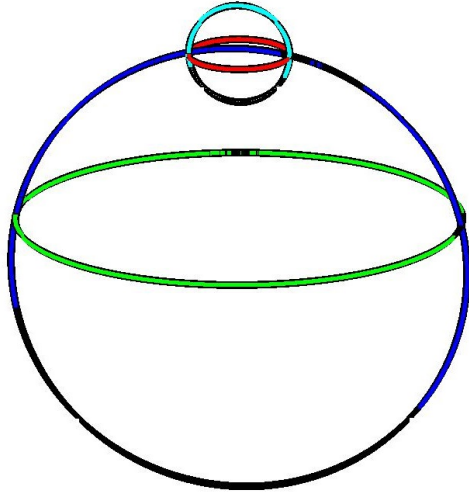


Figure 13. Arm calibration

7.3. Additional Analysis Figures

7.3.1 Additional Histograms

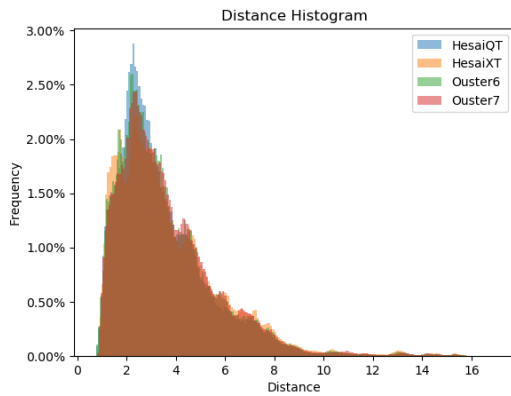


Figure 14. Distance Histogram

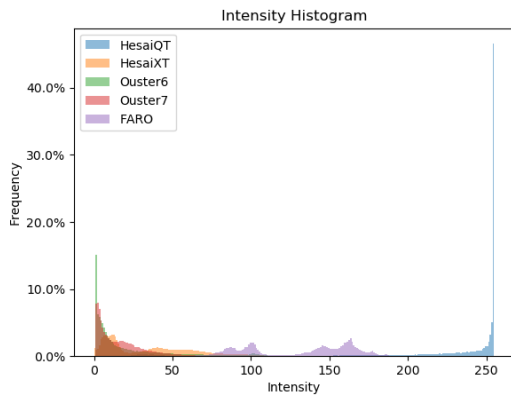


Figure 15. Intensity Histogram

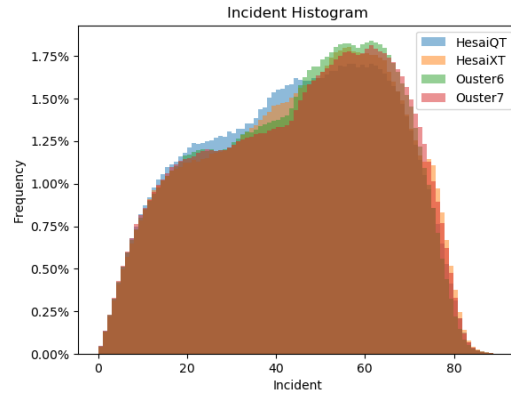


Figure 16. Incident Histogram

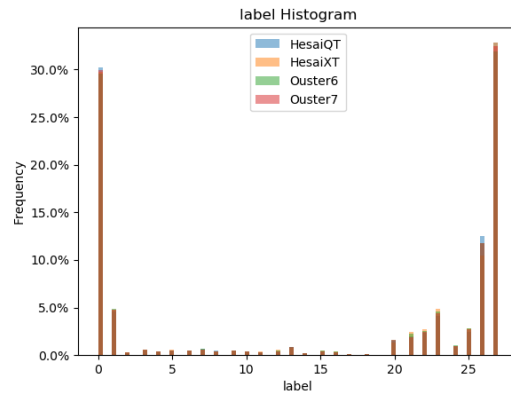


Figure 17. Label Histogram

The distance histogram shown in Figure 14 illustrates the distribution of measured distances, with a noticeable peak between 1 to 6 meters across all LiDAR models, followed by a gradual decline at greater distances. This indicates a common operational range preference among the tested indoor LiDARs.

Figure 15 displays the intensity histograms. Notably, the HesaiQT LiDAR exhibits a sharp peak at maximum intensity, in contrast to the other models, which follow a logarithmic response pattern, suggesting differences in intensity encoding for different LiDAR.

The Incident Histogram, shown in Figure 16, reveals a broad distribution of incident angles, with a concentration between 10 and 70 degrees.

The Label Histogram, shown in Figure 17, presents the frequency distribution of assigned labels, with significant peaks at labels 0 and 25 showing they are more common in the environment.

7.3.2 Accuracy Analysis by Distance

Figure 20 presents a boxplot of accuracy across different distance intervals for the four LiDAR systems. The data

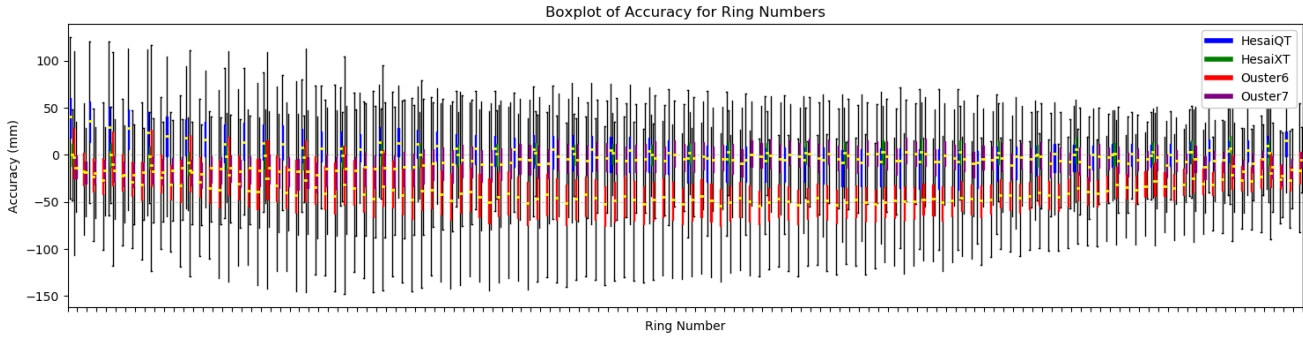


Figure 18. Ring vs Accuracy

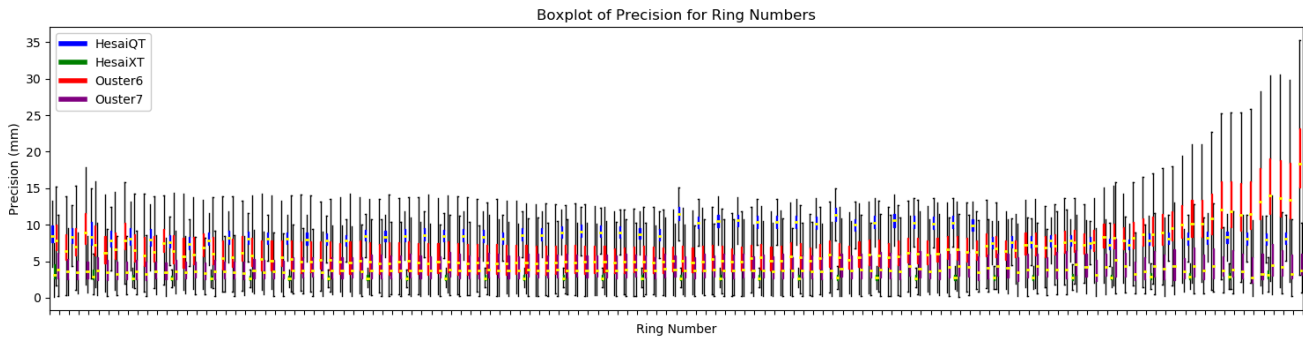


Figure 19. Ring vs Precision

shows substantial variability in accuracy at the closest and farthest distances, likely due to a reduced sample size at these extremes. However, within the range of 0 to 17 meters, there is no significant trend in accuracy, indicating consistent performance across most distance intervals.

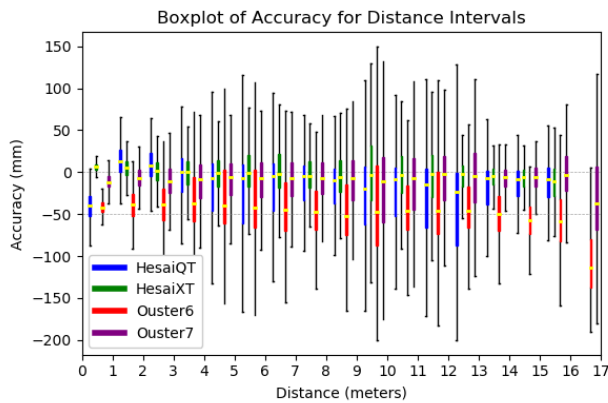


Figure 20. Distance vs Accuracy

7.3.3 Ring Number Analysis

Figure 18 presents a boxplot of accuracy across ring numbers. The plot reveals that for HesaiQT and Ouster6, there are fluctuations of several centimeters in accuracy with the

ring number. The fluctuations of accuracy for Ouster show a pattern of groups of four. This might be related to the design of the sensors.

The corresponding precision analysis, shown in Figure 19, reveals less fluctuation compared to accuracy, with variations typically within a few millimeters. Notably, the Ouster6 exhibits poorer precision in higher rings, while the HesaiQT demonstrates reduced precision in the middle regions of certain rings, potentially reflecting sensor-specific design factors.

7.3.4 Accuracy Analysis by Label

Figure 21 illustrates the distribution of accuracy across various labels, sorted by Faro intensity, which correlates to specific object types. Some labels exhibit broader accuracy spreads, suggesting that certain materials or surface characteristics present greater challenges for precise LiDAR measurements. This highlights the need to account for environmental factors in the deployment and calibration of indoor LiDAR systems.

7.3.5 Accuracy Analysis by Intensity

Figure 22 depicts a boxplot of accuracy for intensity intervals, again comparing the four LiDAR systems. Among the systems, HesaiXT is relatively stable. HesaiQT fluctuates

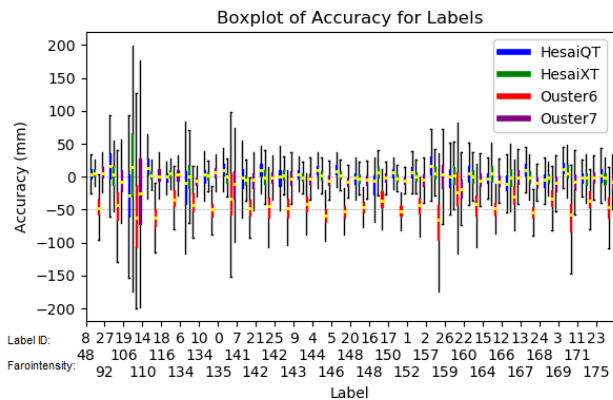


Figure 21. Label vs Accuracy

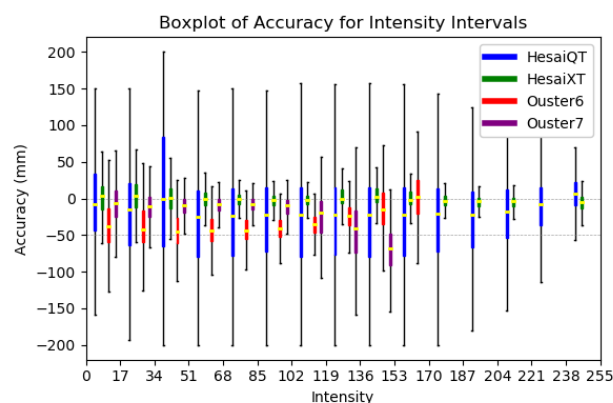


Figure 22. Intensity vs Accuracy

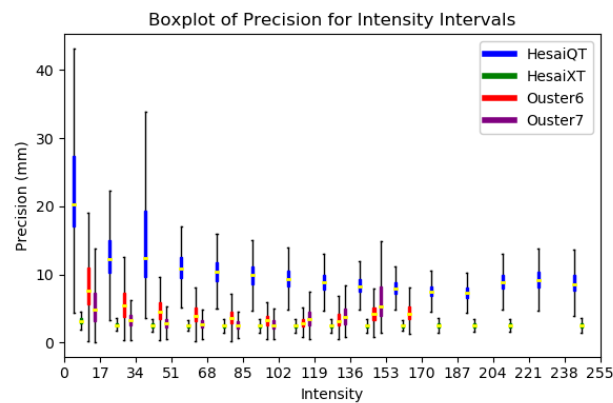


Figure 23. Intensity vs Precision

greatly at lower intensities and there seems to be a slight trend towards reduced variability in accuracy as intensity increases. Ouster7 shows a negative offset as intensity increases, while Ouster6 shows a positive offset as intensity increases.

Figure 23 focuses on the precision of measurements across intensity intervals. The boxplot reveals that precision generally improves as intensity increases for all four

systems. The HesaiQT system exhibits notably higher precision variability, especially at lower intensities, compared to the other systems.

7.3.6 Chessboard Results



Figure 24. Chessboard Ground Truth Mesh

In our analysis, we designed a setup that includes two calibration boards placed within the scene to evaluate the accuracy and precision of different LiDAR models under controlled conditions. Figure 24 illustrates the setup, featuring one board for color and grayscale calibration and another with a black-and-white checkerboard pattern. Both boards are constructed from the same material but have different surface coatings, which result in varying levels of reflectivity and consequently impact LiDAR performance. The following figures display point clouds that are color-coded based on the accuracy and precision metrics derived from the LiDAR scans. In the precision figures, red denotes poor precision, while green indicates higher precision. In the accuracy figures, relative to each LiDAR’s average accuracy, blue signifies a negative offset, red indicates a positive offset, and green represents values close to the average accuracy.

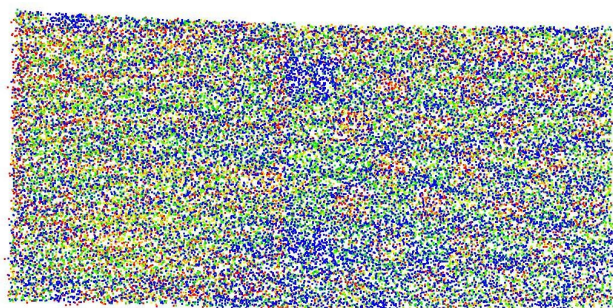


Figure 25. HesaiQT Accuracy

For the HesaiQT LiDAR, as shown in Figures 25 and 26, the accuracy results indicate that the white squares of the checkerboard yield measurements that are closer to the median accuracy value, whereas the black squares exhibit both positive and negative deviations from the median. Precision measurements do not exhibit a clear trend across the

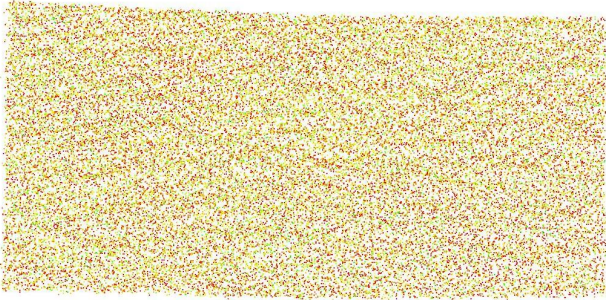


Figure 26. HesaiQT Precision

checkerboard pattern, indicating variability in precision that does not strongly correlate with the checkerboard's color.

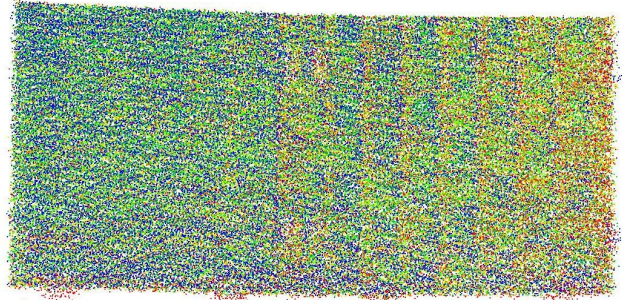


Figure 29. Ouster6 Accuracy

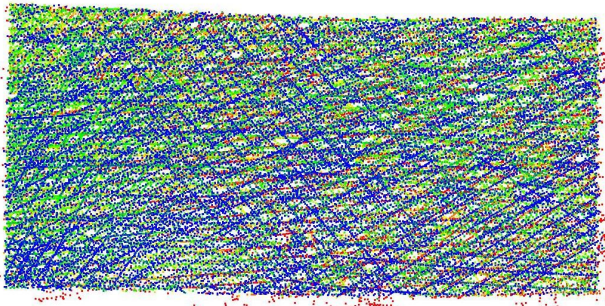


Figure 27. HesaiXT Accuracy

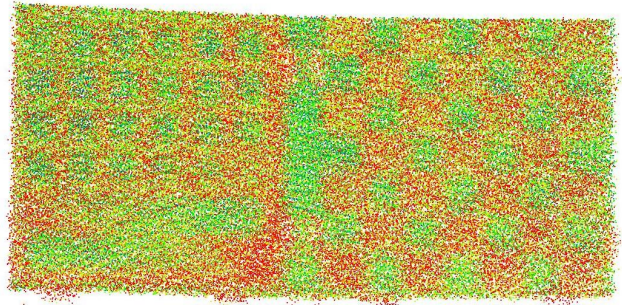


Figure 30. Ouster6 Precision

precision. This suggests that the Ouster6 LiDAR's performance may be influenced by the surface properties of the calibration board.

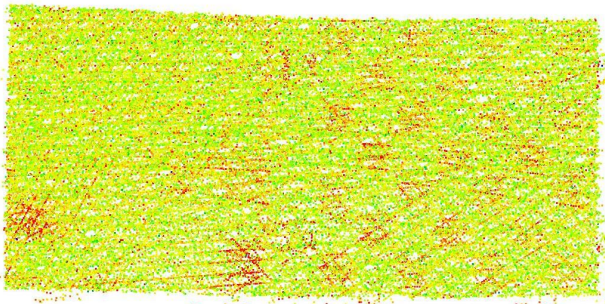


Figure 28. HesaiXT Precision

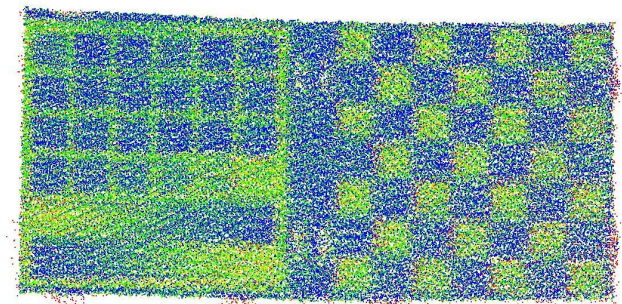


Figure 31. Ouster7 Accuracy

Figures 27 and 28 present the results for the HesaiXT LiDAR. Here, we observe that the accuracy for the black squares is higher and closer to the median, while the white squares tend to show a negative deviation. In terms of precision, the black squares display poorer precision compared to the white squares, suggesting that the surface characteristics of the black squares may introduce more noise or uncertainty in the measurements.

For the Ouster6 LiDAR, depicted in Figures 29 and 30, a certain grid pattern can be discerned in the accuracy data, although no dominant trend is evident. Precision measurements indicate that the black squares have relatively poor precision, whereas the white squares demonstrate better

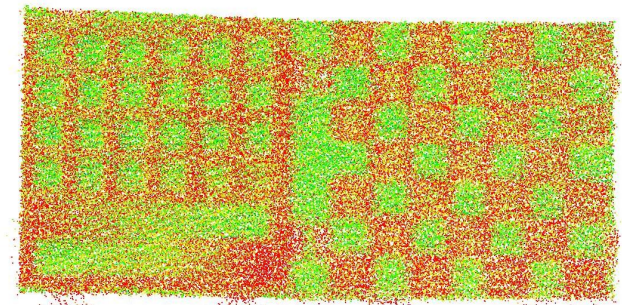


Figure 32. Ouster7 Precision

Lastly, Figures 31 and 32 show the results for the Ouster7 LiDAR. Similar to the HesaiXT, the accuracy measurements indicate that the black squares have higher accuracy and are closer to the median, while the white squares exhibit a negative offset. In comparison to the precision results of the Ouster6, the Ouster7 displays similar trends; however, the boundaries in the precision data for the Ouster7 are more distinct, suggesting reduced point cloud noise.

These results underscore the importance of considering the material properties and surface characteristics in the evaluation of LiDAR systems, as these factors can significantly impact both accuracy and precision in indoor environments.

7.4. Dataset Access and Usage

The complete dataset, including raw LiDAR scans, ground truth data, and pointclouds with associated metadata, will be available at <http://lidaraccuracy.github.io>. The dataset is organized into several folders, providing both raw and processed data:

- **rosbag**: Contains raw LiDAR scans in ROS bag format.
- **result**: Includes processed point clouds with metadata after raycasting.
- **pose**: Provides static point cloud poses.
- **groundtruth**: Comprises ground truth FARO point clouds and labeled meshes.
- **armtf**: Contains raw arm pose data in CSV format.
- **opti**: Includes raw OptiTrack pose data in CSV format.
- **scripts**: Offers sample code for loading and processing the data.

We encourage researchers to utilize this dataset to advance the development and validation of LiDAR calibration methods, SLAM algorithms, and 3D reconstruction techniques. The dataset's comprehensive nature and meticulous organization make it a valuable resource for pushing the boundaries of indoor LiDAR performance analysis.